The Electronic Conference on Pharmaceutical Sciences
ECPS2011

sciforum
e-conferences
www.sciforum.net

Communication

Two Dimensional orthogonal imaging of laminar fluid flow across API surface: Insight into dosage concentration inside GI Lumen and permeability

James Lenke [1,*]

[1] Paraytec, Ltd. / 1a St. Georges Place, York, UK

E-Mails: jim.lenke@paraytec.com (Jim Lenke)

* Author to whom correspondence should be addressed; Tel.: +44-(0)1904 526270; Fax: +44-(0)1904 652101

Received: 18 Feb 2011 / Accepted: / Published:

Abstract: Historically, dissolution devices have been performing measurements away from the solid-liquid interface and then drawing conclusions. Simply relocating measurements to this interface using a 2 dimensional imager, recording absorbance intensity over time of laminar flow across the sample surface, opens significant insight about the concentration gradient at the surface, in-situ surface pH, and unique insight of bioavailability. Having this information early in development provides formulators with better insight into optimum form.

Keywords: 2 Dimensional imaging, in-situ surface pH; solid-liquid interface; poorly soluble; boundary layer, dynamic solubility, bioavailability, linear velocity.

---

1. Introduction

Dissolution of API material from a surface is an important characteristic measurement used in conjunction with solubility to determine an appropriate dosage. Intimate understanding of the dissolution process at the solid liquid interface is not possible with traditional equipment which leaves many problems with product development, particularly poorly soluble compounds. This development cycle quite often suffers from too little information too late. Surface imaging of a laminar flow-through cell offers a tremendous amount of information for development teams from synthesis through first in trials. First introduced in 2008[1], UV imaging coupled with laminar flow is able to generate 4-

dimensional data from absorbance intensity over a 2-dimensional area over time. When this technique is applied to dissolution [11] it offers incredible information about the solid-liquid interface such as static diffusion rate, boundary layer thickness, boundary layer slope, dynamic solubility, surface solubility, in-situ surface pH, and kinematic viscosity. The minute sample and buffer amounts of 3 – 10 mg and 5 – 10 ml, respectively, analyzed over 10-15 minutes make this incredibly attractive to early stage development [3, 4, 5]. Likewise, pharmacokinetics will appreciate a specially designed micro flow cell (1/10 the diameter of the small intestine) that maintains laminar conditions over a volumetric and linear velocity range equivalent to published Human SI rates [4, 6, 22]. With the Reynolds number and flow rate similarities, it is not much of a stretch to consider the small sample surface area as a 1mm particle API situated on the Villi surface of the Lumen. Such rich information from small amounts of sample will be appreciated by all researchers.

2. Results and Discussion

Theoretical understanding of fluid dynamics of laminar flow through devices [9,10,16,17,21] has been available for quite some time, and flow through devices are readily used today, but not extensively applied[2]. Laminar flowing devices specialized for small, compressed API powders were investigated thoroughly as early as 1975 for use as an alternative to measure the dissolution process [9, 10]. Since then, very little progress has been made until recently [1, 17]. A laminar flow through device has many benefits that seem to be under appreciated, such as continuous flowing regimes similar to physiological conditions with low Reynolds number, steady state conditions, and continuous supply of buffer[16].

Convective diffusion models and evidence have been thoroughly presented, but overall the technique has failed to successfully gain support as a viable research tool. One possible explanation, which has a similarity to traditional apparatuses, would be disconnected measurements, or analytical measurements at a large distance away from the original reaction leaving a hole for explanations of the detailed process. The obvious cure for this is to move the analytical measurement to the actual solid-liquid interface, which has recently been successfully demonstrated [1, 11].

Convective diffusion of a laminar flow through device was thoroughly characterized by Nelson and Shah[9]. The predicted diffusion rate could be derived based on parameters of the compound, fluid flow, and device dimensions. This is seen in Eq. 1 where DR is diffusion rate, D the diffusion coefficient, S the maximum solubility, α represents the shear rate, and w, L the cell width and length respectively[17]. Whereas in a 2-dimensional imager a mass flux is measured to provide the intrinsic dissolution rates (IDR) based on downstream measurements in a detection zone using Eq. 2. Briefly, a measurement zone defined as a fixed width vertical column containing hundreds of rows of pixels, records material transported downstream through each row of pixels. The mass in each pixel is obtained from the molecular weight and extinction coefficient as applied in Beer's law. The mass flux is corrected by pixel row away from the surface for the velocity in that plane using Eq. 3 to accommodate faster velocities in the central flow stream and near zero flow at the surface. Nominally, Q is flow rate, h the cell height, w the cell width and Z the pixel row height above the surface.

$$DR = 0.808 \cdot D^{\frac{2}{3}} \cdot S_{max} \cdot \alpha^{\frac{1}{3}} \cdot w \cdot L^{\frac{2}{3}} \quad (1)$$

$$J = \frac{\sum_{z=0}^{H/2} v_Z \cdot M \cdot c_Z \cdot w \cdot \Delta Z}{A_{surface}} \quad (2)$$

$$v_Z = \frac{3Q}{2hw}\left(1 - \frac{(2Z-h)^2}{h^2}\right) \quad (3)$$

$$dS = \frac{DR}{Q} \cdot \left(\frac{c_{width} \cdot c_{height}}{s_{width} \cdot s_{length}}\right) \quad (4)$$

Fluid flow into the flow cell, Fig 2b, is controlled through a high accuracy, variable rate dual position syringe pump pushing fluid inside a stainless tube connected to a heating element to raise the temperature of the buffer prior to entering the flow cell. The elliptical shape of the flow cell, seen in Fig 2 (c) has been carefully designed to provide a laminar flow throughout the entire cell. Internal volume of the flow cell is approximately 0.5 ml with internal dimensions at the centre of 4.0 mm wide x 3.5 mm high. This cross sectional area was chosen based on dimensions of the camera chip, but also to offer a 1/10 model of the small intestine published to be 3.5 cm diameter. Fluid pumping can also be managed by a standard HPLC pump where it can be realized that a constant flow of increasing pH gradient can be put through the cell to collect IDR at several pH in one experiment, which has the benefit of easily mimicking the pH change of the GI tract. Further to this, because the cell volume is small, rapid flow rate changes can be easily managed with the ability to go from high velocity (2.0 ml/min) down to no velocity (0.0 ml/min) instantaneously without any ill effects.

Many additional benefits are available from a small flow through system. For a total experiment of 12.5 hrs a mere 150 ml of buffer would be used, which is very beneficial when using biorelevant media (See Table 2). From Table 1 a flow rate of 0.2 ml/min corresponds to nominal published physiological linear velocities, 1.3 – 1.5 cm/min [6, 22] (or 0.25 mm/sec) which is approximately 18 sec to move across the face of the detector. Further, effluent collected for 5 minutes, at this flow rate, would offer 1 ml of solution, which is a manageable volume for direct use with permeability systems such as PAMPA or Caco-2. The effluent concentration can be estimated by dividing the measured IDR by the flow rate to arrive at a concentration (mg/ml), which must be corrected for the ratio of cell cross sectional area to sample area as in Eq. 4. This concentration is the solubility in a dynamic system, or the *dynamic solubility* (dS) and its relationship to IDR and flow rate are seen in Fig. 1.

Table 1. Linear velocity (cm/min) comparison of flow through cells from volumetric flow rate and cross sectional area.

	Sectional area (cm^2)	**0.14**	**11.3**	**22.6**
Flow rate (ml/min)	0.1	0.7	0.1	0
	0.2	**1.4**	0.2	0
	0.4	2.9	0.4	0.1
	0.8	5.7	0.8	0.2
	1.2	8.6	**1.2**	0.3
	2.0	14.3	2.0	0.5
	4.0	28.6	4.0	**1.0**
	8.0	57.1	8.0	2.0
	16	114	16.0	4.0
	32	227	32.0	8.0

Table 2. Volume (L) of buffer used for each cell size based on linear velocity of 1.2 cm/min taken from Table 1 above.

	Time (min)	**60**	**270**	**420**	**Total(L)**
Area(cm^2)	Flow rate (ml/min)				
0.14	0.2	0.012	0.054	0.084	0.15
11.3	1.2	0.072	0.324	0.504	0.90
22.6	4.0	0.240	1.08	1.68	3.0

Figure 1. Data from a poorly soluble compound showing relationship between dynamic solubility and IDR vs. flow rate.

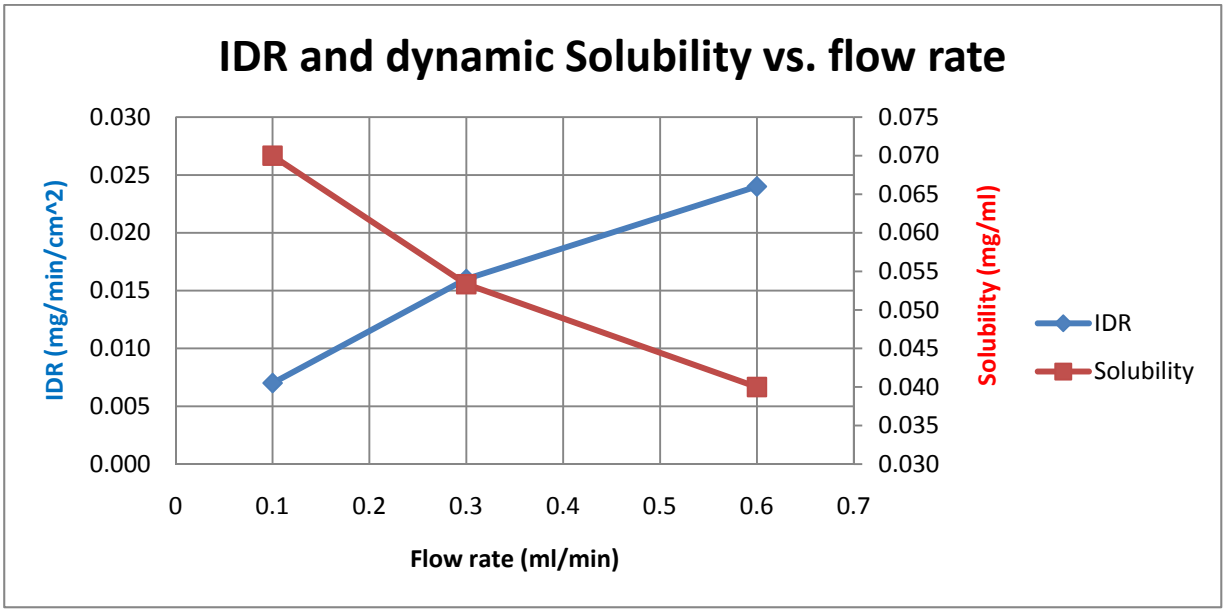

2.1. 4-Dimensional data from a 2- Dimensional UV detector

A parallel pixel array, which has many similar properties to a digital camera, offers an impressive amount of data when trained on a reaction zone such as a solid-liquid interface. Resolution and orientation of image relative to the reaction zone are explained in Fig 2. With each pixel acting as an individual UV detector, an unparalleled level of temporal and high resolution spatial data directly of the solid-liquid interface is now available. Relocating measurement of the dissolution process offers insight into previously hypothesized surface events such as surface pH, boundary layer thickness, and concentration gradient. However, further data can be collected on static diffusion rate, boundary layer gradient, surface concentration, dynamic solubility, and surface changes from swelling or gelling.

The 4 mm optical path length offers a good range of sensitivity, especially for very poorly soluble compounds. Before dissolved material has been allowed to dilute, the highest concentration achievable from a poorly soluble compound is directly at the surface. Indeed, experience with a variety of very poorly soluble API compounds shows that those unable to be detected have a physical change at the surface preventing detection. By selecting the corresponding chromophore wavelength, the concentration can be tracked in the immediate vicinity of the sample. This advantage is used for measurement of surface pH described below.

The sensitivity and positional accuracy available to Ketoprofen, a poorly soluble compound investigated often [3,5,7,8], is displayed in Fig 3. Using preferred flow rates from above, the 0.1 and 0.3 ml/min profile lines in Fig. 9 show the distance to which this compound will be carried into the flow stream and the concentration at the surface. These profile plots are created from any of three vertical measurement wands that can be placed along the X axis relative to the sample surface as desired. Thus, profiles can be found directly over the center or further downstream.

Figure 2. (a) Diagram of parallel pixel array showing overall viewing area and pixel dimensions. **(b)** Cartoon diagram of imaging system operation. Single wavelength light enters the flow cell (A) while fluid is pumped into the cell (B) at predefined rates, transmission is recorded by the camera chip behind the flow cell (C). Waste effluent leaves the flow cell downstream (D) from the sample surface (E). Geometrically, the sample surface is parallel to the buffer flow but perpendicular to the light and camera creating a 4 dimensional array (X,Y, Intensity, time) used to extract data in and around the solid-liquid interface. **(c)** Cartoon diagram showing fluid entering at the left across the sample, solid red square in the center, with the diffuse stream to the right being the dissolved mass exiting. Fig 2 (b) – C- camera chip, would be located behind the red sample with light entering in front.

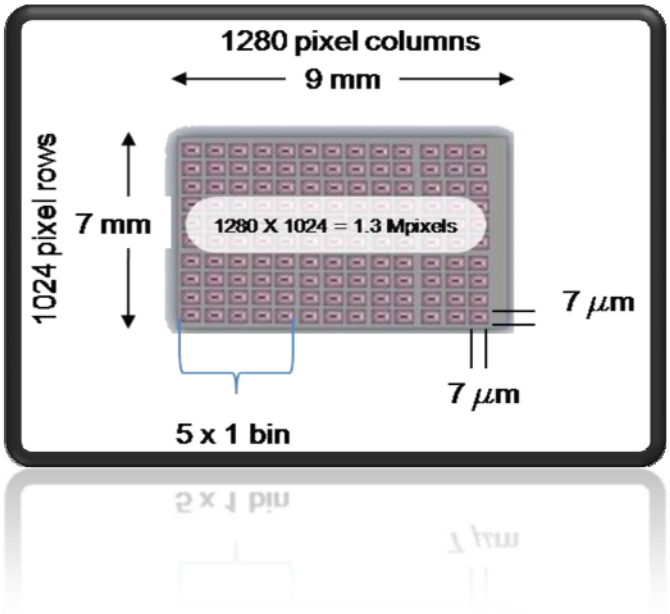

[A]

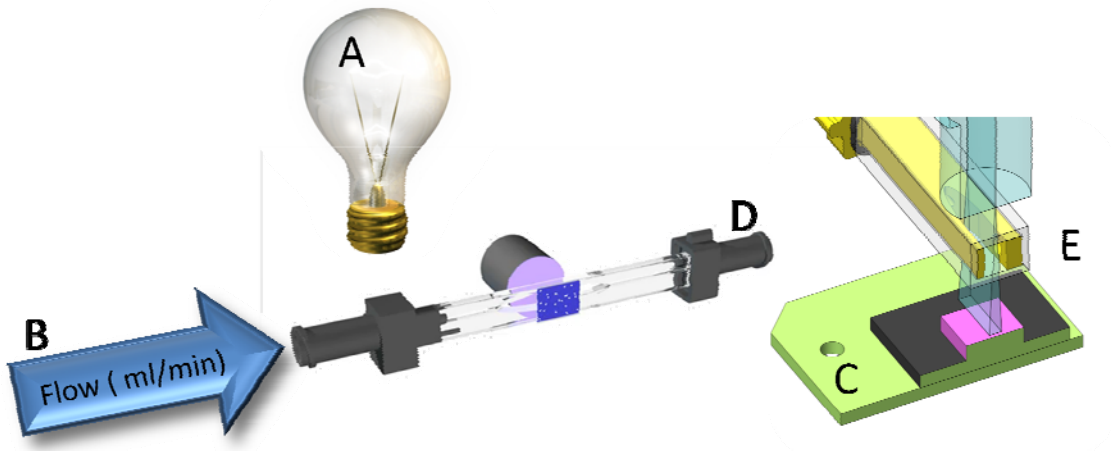

[B]

[C]

Figure 3. (a) Actual image (false colored) shown next to the imaging area. The Z axis is away from the surface, X left to right and Y axis as depth. Horizontal viewing area of the chip is fixed at 9 mm, but the viewing height (Z) can be adjusted depending on data collection rate and required resolution.

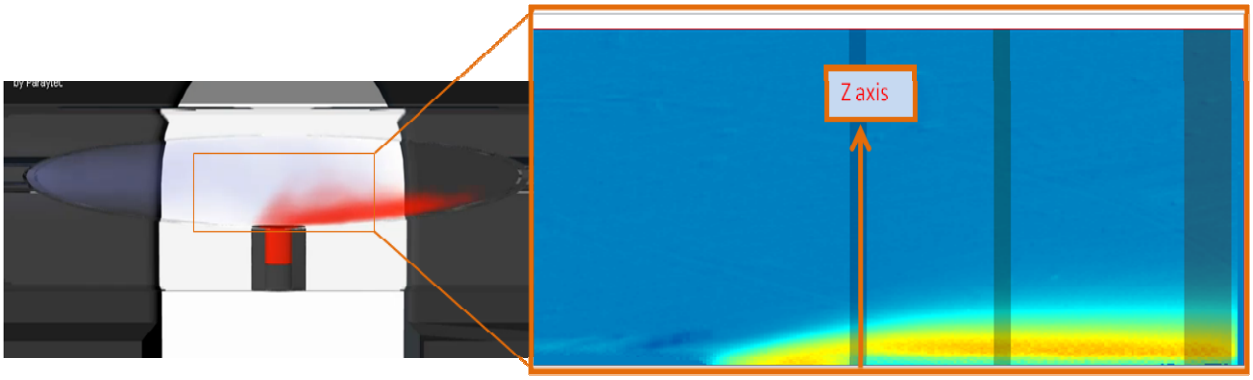

2.2. in-situ Surface pH measurement

It has been known that the pKa of compounds can influence the bulk pH [5, 7, 12, 13, 14]. Equally so, it has been known that the boundary layer is the driving force behind the dissolution rate. From a practical point of view, the more material transferred from the surface to the bulk solution the higher the absorbance. Thus determining either the best salt form to control the in-situ surface pH or excipients to increase the boundary layer will improve the dissolution rate of the API in question. Herein lays the origin of designing supersaturated solutions of poorly soluble compounds to influence the rate of material leaving the surface.

Measurement of the surface pH depends on the difference between the compound pKa and buffer pH and the matching of the pKa to the indicator dye. Less than 2 pH units are difficult to measure, and optimally the indicator dye range should span the pKa. In the case of Ketoprofen, Methyl Red (MR) diluted solution was prepared using the pH 6.8 buffer. All pH indicator dyes change color, and thus absorbance, upon pH change. Fig 4 shows a plot of absorbance vs. pH change for MR. The dilute dye solution is pumped through the cell and the baseline is established with the dye in place.

A calibration of absorbance vs. pH was made previously to coordinate pixel intensity with pH. Previous estimate of surface pH of Ketoprofen has been made [7] using an independent measurement of a saturated bulk solution. The results obtained using a pH indicating dye is in good agreement, Fig 5.

A similar experiment was conducted on Atenolol, a rapidly soluble compound with a pKa of 9. It is known that compounds such as this can alter the bulk solution pH. In this instance, with relatively low volumetric flow (0.3 ml/min) the density of the high pH solution was too heavy to remove out of the flow cell and was pulled down with gravity, Fig 6. This raises questions about the concentration at the surface. Similar high pKa compounds such as Vancomycin exhibit similar properties and performance seen in Fig 7.

Figure 4. (a) Diagram showing dye solution pumped across sample surface. **(b)** Plot showing pH vs absorbance with the arrow indicating decreasing pH.

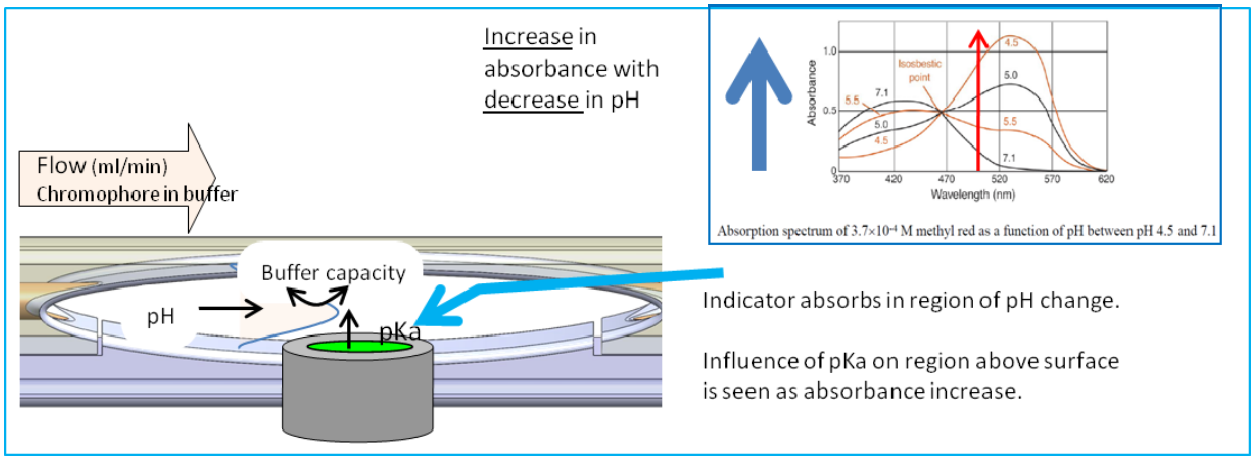

Figure 5. (a) UV absorbance data image showing intensity and distance of coverage for Ketoprofen in water. Contour lines are present in the image and represent every 100 mAU **(b)** Estimated pH based on calibration curve of Ketoprofen in water. Note smaller absorbance area compared to UV image.

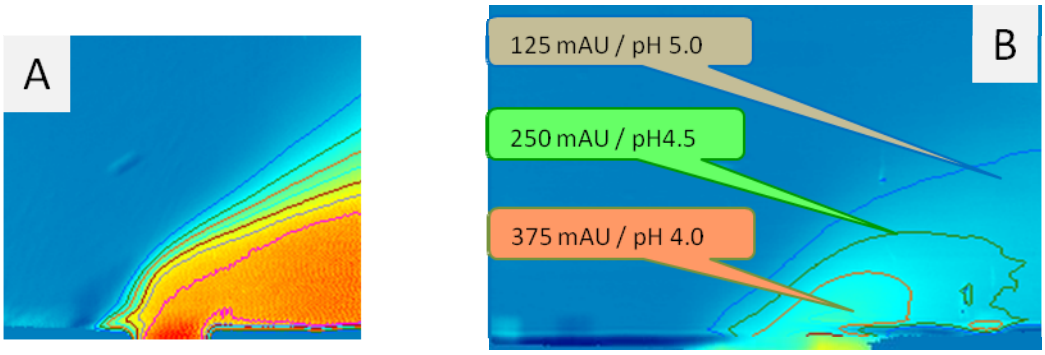

Figure 6. (a) Data image of Atenolol in pH 4.5 buffer at expected wavelength max for Phenolpthalein, however no absorbance appears because a high enough concentration of phenolphthalein was not used. The refractive index change from density gradient is observable. **(b)** UV Data image showing a dense solution layer forming over the sample surface.

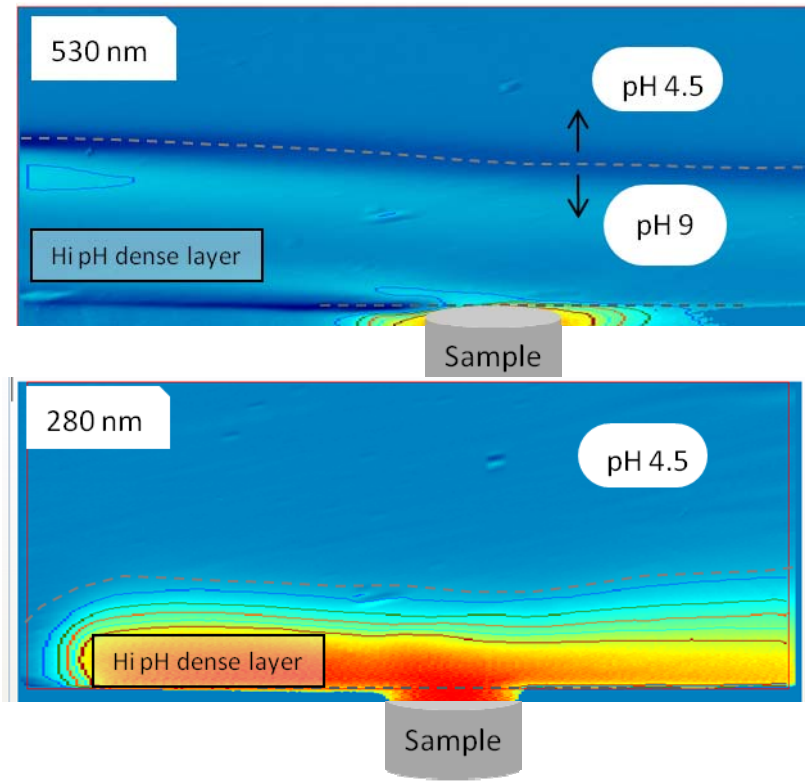

Figure 7. Basic pKa compound Vancomycin exhibiting similar trends as Atenolol. **(a)** Sigma - arrow denotes small concentration gradient **(b)** USP – arrow denotes material removed from shear rate most likely from smaller particle size.

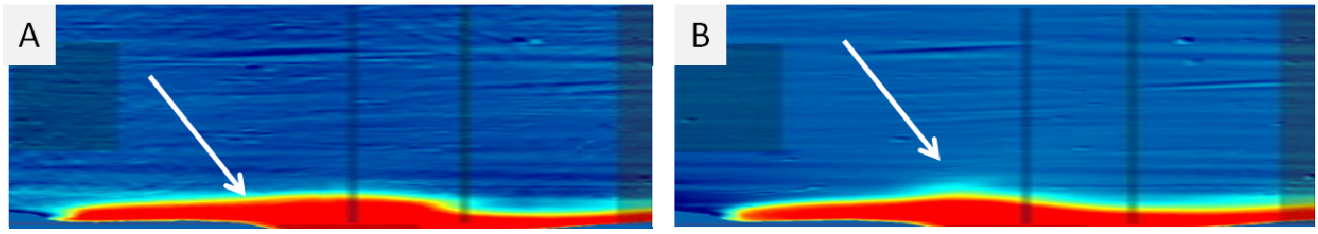

2.3. Boundary layer

Understanding the role of the boundary layer as it applies to both the API and Villi surface is vital to understanding oral absorption.[18] To date this has been very difficult to measure and understand from both the disconnected measurement location and time delay from reaction to measurement. Currently poorly soluble compounds receive a great deal of interest in order to enhance or control the boundary layer. [13, 20] Insight into the values and conditions at the surface can aid greatly in determining not only which form of API, but also solving problems associated with current product batches.

A single data image, such as Fig 8, contains a wealth of information that can be found in the concentration gradient above the surface boundary. Three distinct values can be made for any compound: Surface concentration, slope of concentration gradient and rate at which material leaves the gradient.

The surface concentration is easily found from the average intensity within a defined region of interest (ROI). The volume is the area of the ROI times the path length, and once absorbance value is converted to mass an absolute concentration is known. The slope of the concentration gradient is indicative of ease to which the dissolved material moves into the bulk stream. A more horizontal slope is an easy transition whereas a more vertical slope defines a sharp contrast. Finally the rate of material loss can be found from the difference between two vertical measurement wands at a defined spacing. Using the increase in vertical height of concentration (Z) and the distance between the two wands creates a triangle to which the hypotenuse is the rate loss per linear distance.

Viewing the gradient as a function of flow rate, as in Fig 9, will reveal the extent to which a concentration can move into the bulk flow stream. Further to this, the area under the curve (AUC) is an additional differentiation value between API forms. Work has been carried on stability of the laminar dissolution steady state by comparing differences in AUC over several consecutive time points 1 min apart, which revealed reliable reproducibility.

Figure 8. (a) Plot of absorbance profile over distance showing three different measurement wands located at sample center, 2.5 mm downstream and at the camera edge. **(b)** Data image of Ketoprofen showing the absorbance intensity at various positions. Easily seen are the transitions in the concentration gradient and the high concentration at the surface. **(c)** Zoom of data image.

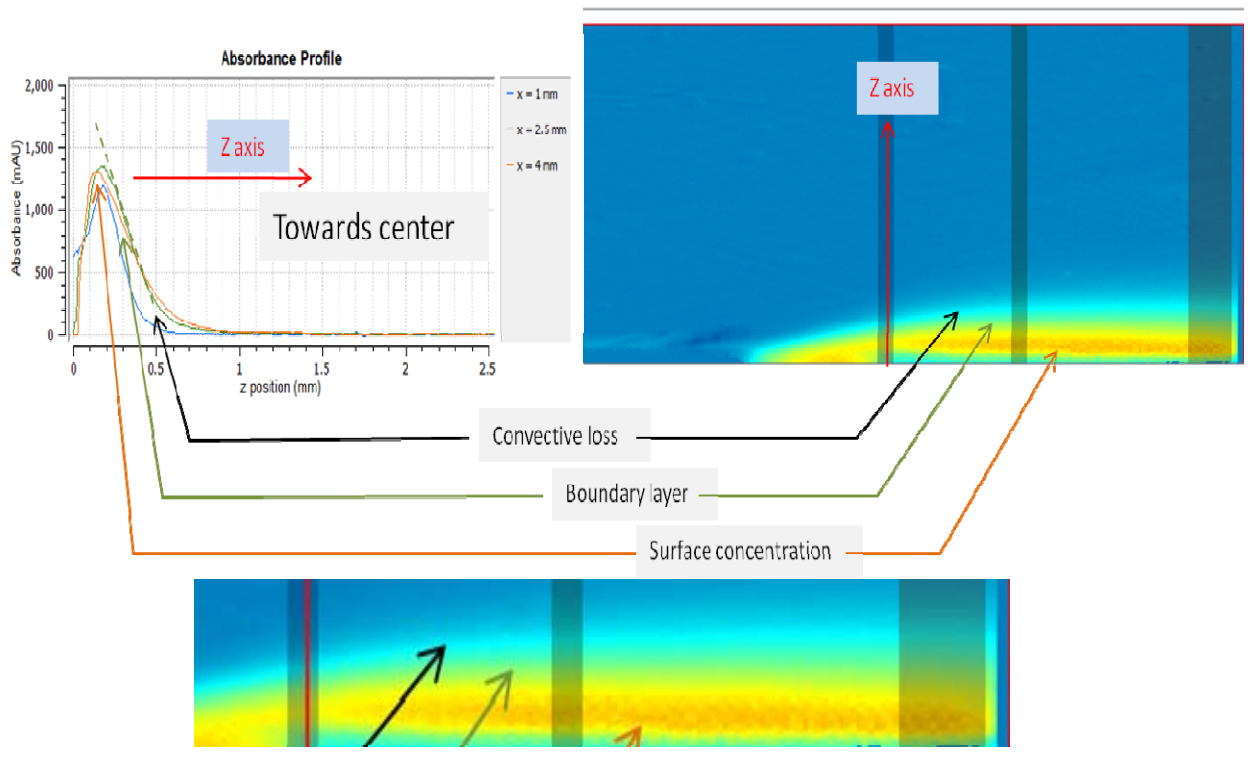

Figure 9. (a) Absorbance profile of Ketoprofen taken from vertical measurement area seen in Fig 8 at various flow rates. The slope of the curves identifies the concentration gradient while the static flow curve shows the distance solution migrates into the bulk solution. The static diffusion rate can be found from the spatial difference of profiles between two time points to offer distance/time (mm/sec).

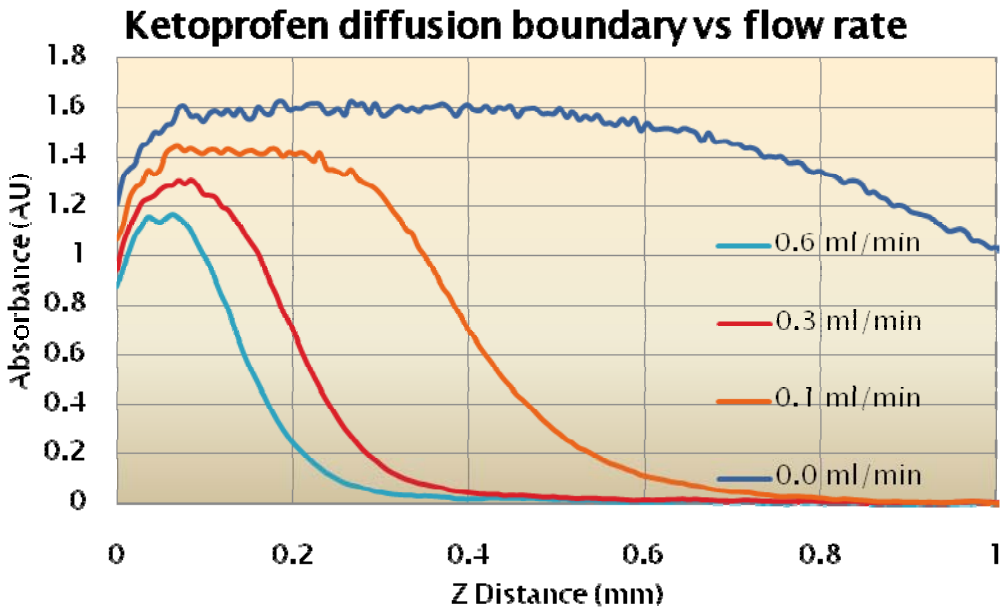

2.4. GI model

The gap between knowledge about physiological conditions, as they relate to dissolution, and dissolution apparatus improvement continues to widen each year leaving researchers with many unanswered problems [15]. The hope has long been for more knowledge, particularly towards predicting in-vivo results earlier [4, 14]. Simulating the GI is complex and not easy. However, a steady state and reproducible model is an excellent starting point.

Starting with the premise that the current flow cell is a 1/10 model of the small intestine and that identical linear velocities are easily obtained, it is a small stretch to imagine the flow cell as a section of the intestine with a camera positioned to look through the wall at the internal flow characteristics. This would resemble the view seen in Fig 10 and 11 where Fig. 10 depicts integration of the sample cup with the intestinal wall. Using the advantage of 2-dimensional data from an area imaging device, it can be seen how convective diffusion carries a finite concentration downstream and from the available measurements described above, what the concentration and pH would be at the Villi surface in this scenario. Of course peristaltic mixing inside the small intestine ensures equal mixing of contents to provide maximum Villi exposure, however, the measurements can be applied in the opposite direction. If a particle is in the middle of the flow stream, static diffusion would take too long to travel towards the Villi surface, therefore mixing would be required to bring the particle closer to the surface, which is similar to the original premise. Regardless of particle location, the in-situ surface pH and surface concentration values would remain the same as measured.

In the case of a particle dissolved upstream, a concentration plug entering the observation zone would show diminishing concentration at the surface with higher flow rates as previously explained. [19] Data images at different flow rates of identical injections of Caffeine, Fig 12, reveal the thickness of the aqueous boundary layer and concentration per time entering this zone. In this case, for a discrete finite volume of plug, the 2-dimensional data can show concentration at the surface over time, which when applied to the total internal surface area can provide a measure of available concentration rate for a given inlet concentration (dosage). This model system is novel and can offer significant advantage if correlation with in-vivo results can be realized as.

Figure 10. (a) Cartoon diagram showing location of API 'sitting on' wall of small intestine with flow passing across the surface and transporting material downstream. Offline analysis shows both the concentration immediately downstream of the sample and the rate plus amount lost into the central flow stream from convective diffusion. A compressed sample 2.0 mm diameter is equivalent to a 1 mm particle.

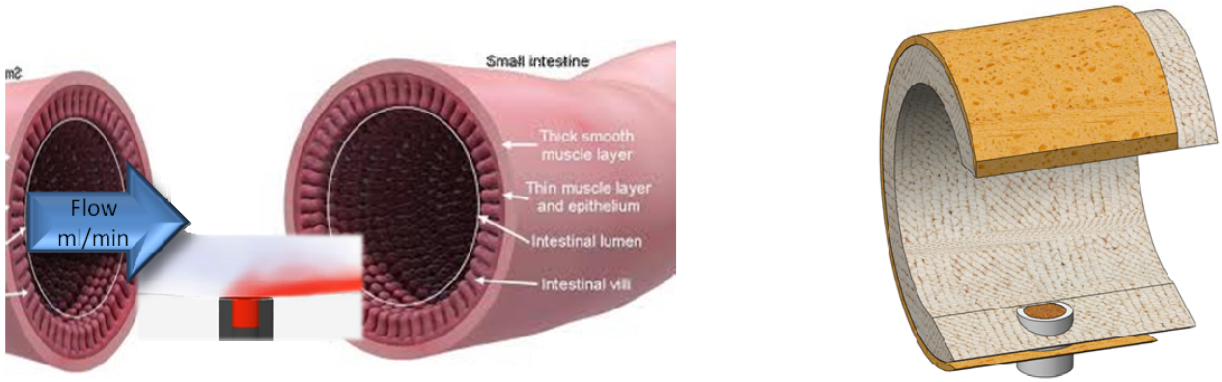

Figure 11. (a) Side profile view of fluid flow inside a tube, representing model scenario in small intestine adapted from (19). Shown are the values for flow in (Q_{in}), concentration (C_{in}) (C_{out}), and boundary layer thickness ($\delta_{boundary}$), which is a function of flow rate. Higher rates will have a thicker layer.

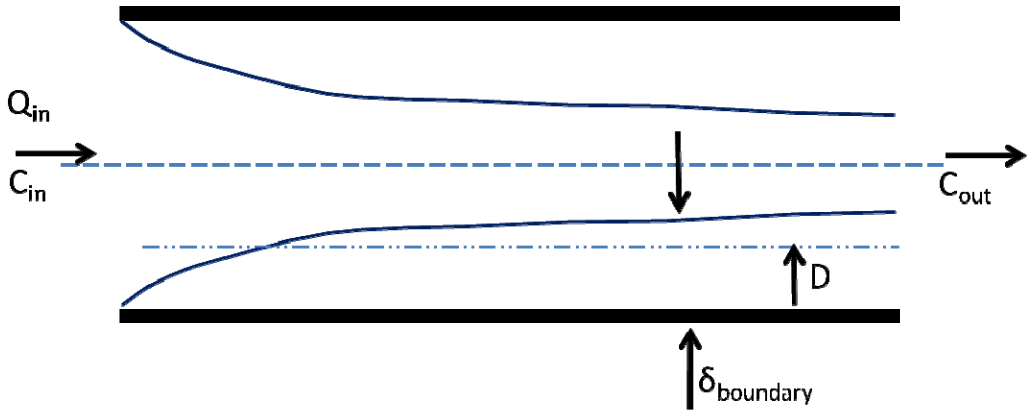

Figure 12. (a) Injections of caffeine showing how radial distribution is affected at different flow rates. Worth noting is the varying thickness of the stagnant layer seen in all images, which corresponds to $\delta_{boundary}$ seen above.

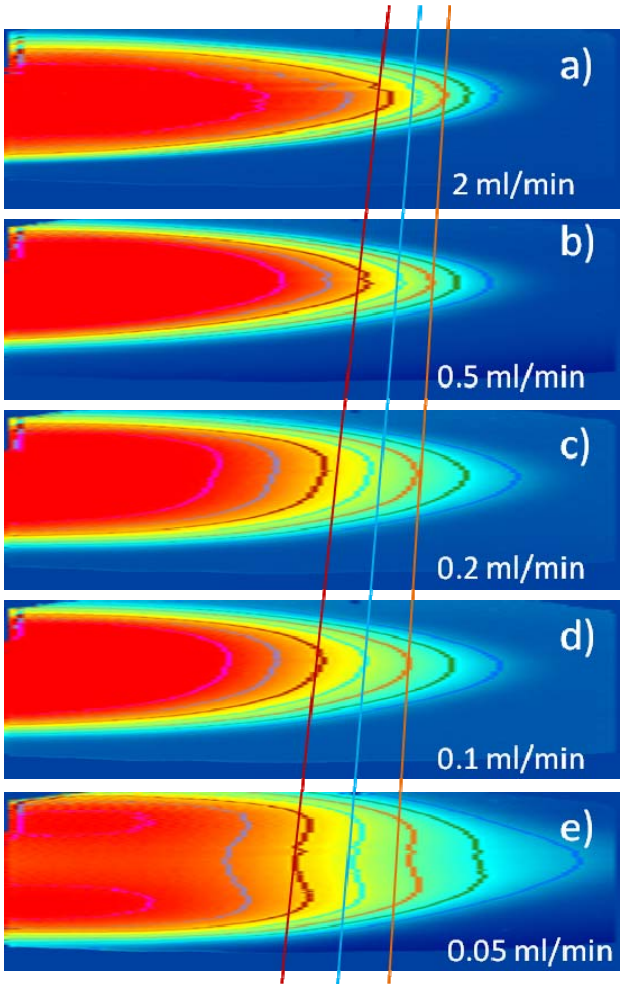

3. Experimental Section

Materials:

Chemicals: Griseolfulvin (Sigma G4753), Ketoprofen (Sigma K1751), Atenolol (Sigma A7655), Methyl Red (Sigma M7267); Phenolpthalein (Sigma P9750), Vancomycin (USP), Vancomycin (Sigma)

Buffers: SGF pH 1.2, SIF pH 6.8, blank FeSSIF pH 5.0
pH Dyes: Methyl Red with pH 6.8 buffer.
Phenolphthalein pH 6.8 buffer.

Eppendorf PCR tubes (Sigma Z316121)
ActiPix© SDI 300 surface dissolution imager (Paraytec SDI 300)
Actipress (Paraytec 342-0000)
Sample cup (Paraytec 341-0009) (2.0 mm ID x 2.4 mm H – 316 SS)
Wavelength 254, 280, 530 nm (Paraytec)

Method:

Sample Prep: All samples were pre-weighed to approximately the same value (5-6 mg) in a PCR tube. The contents of each tube were then emptied into a hand held sample press and compressed under identical torque (40 cNm) for equal times (30 sec) in a re-usable sample cup (316SS 2.0 mm ID x 2.4 mm H). Photomicrograph images were taken of each sample prior to running to ensure a smooth and level surface. The sample cup was then set aside for introduction into the flow cell after baseline subtraction.

System operation: Prior to each run, the appropriate wavelength filter was inserted according to the absorption maximum of the corresponding compound. For all UV analyses the temperature was set for 37 C inside the flow cell, whereas room temperature was used for all pH measurements to avoid altering the dye performance.

Analysis: All results were analyzed using offline software and in some cases the waste effluent was analyzed independently on a UV/VIS spectrometer.

4. Conclusions

It has been shown that relocating measurement to the solid-liquid interface using a 2-dimensional parallel array imager can provide a significant amount of information about the dissolution process. The location of the imager in the flow cell can also provide some understanding of in-vivo conditions towards closing the gap between *in-vitro* and *in-vivo* correlation. It is believed that this technique provides early insight from small amounts of material in biorelevant conditions to support researchers in early API product development.

Acknowledgements

The author sincerely thanks the FDA (DPQR) for supplying Vancomycin material and data along with discussions relevant to this compound. The author wishes to acknowledge with great appreciation the helpful advice and criticism on many topics from Prof. Jesper Østergaard, Copenhagen.

References and Notes

1. Wren, S.A..; Goodall, D.; Lenke, J.; Moon, K.; Swarbrick, M.; Chapman, A.; J. *Pharm. Pharmacol*., **2009**, 61S1, A110.
2. Sinko, P.; *Martins Physical Pharmacy and Pharmaceutical Sciences*, International 6th Ed. Publisher: Wolters Kluwer, London, England. 2009.
3. Avdeef, A.; Solubility of sparingly-soluble ionisable drugs. *Adv. Drug Delivery Reviews* **2007**, 59, 568-590.
4. Hörter, D.; Dressman, J.B. Influence of physiochemical properties on dissolution of drugs in the gastrointestinal tract. *Adv. Drug Delivery Reviews* **2001**, 46, 75-87.
5. Avdeef, A.; Tsinman, O., Miniaturized rotating disk intrinsic dissolution rate measurement: Effects of buffer capacity in comparisons to traditional Wood's apparatus. *Pharm. Res.* **2008**, 25, 2613-2627.
6. Macheras, P.; Reppas, C.; Dressman Estimate of volume/flow ratio of gastrointestinal (GI) fluids in humans using pharmacokinetic data. *J. Pharm. Res.,* **1990**, 7,518-522.
7. Sheng, J.J.; Kasim, N.A.; Chandrasekharna, R.; Amidon, G. Solubilization and dissolution of insoluble weak acid Ketoprofen: Effects of pH combined with surfactant. *Eur. J. Pharm. Sci.* **2006**, 29, 306-314.
8. Yu, L.; Carlin, A.; Amidon, G.; Hussain, A. Feasibility studies of utilizing disk intrinsic dissolution rate to classify drugs. *Int. J. Pharmac*. **2004**, 270, 221-227.
9. Shah,A.; Nelson,K. Evaluation of a convective diffusion drug dissolution rate model. *J. Pharm Sci.* **1975**, 64, 1518-1520.
10. Missel,P.J.; Stevens,L.E.; Mauger,J.W. Re-examination of convective diffusion/drug dissolution in a laminar flow channel: Accurate prediction of dissolution rate. *Pharm. Res.,* **2001**, 24, 2300-2306.
11. Østergaard, J.; Meng-Lund, E.; Larsen, S. W.; Larsen, C.; Petersson, K.; Lenke, J.; Jensen, H.; Real-time UV imaging of Nicotine release from transdermal patch. *Pharm. Res.* **2010** DOI 10.1007/s11095-010-0257-9.
12. Ozturk, S.; Palsson, B.; Dressman, Dissolution of Ionizable Drugs in Buffered and Unbuffered Solutions *J. Pharm. Res*. 5 (1988), 272-282.
13. Hawley.M.; Morozowich, W. Modifying the diffusion layer of soluble salts of poorly soluble basic drugs to improve dissolution performance. *Mol. Pharm.* **2010**, 7, 1441-1449.
14. Sugano,K.; Okazaki, A.; Sugimoto, S.;Tavornvipas,S.; Omura,A.; Mano, T., Solubility and dissolution profile assessment in drug discovery. *Drug Metab. Pharmacokinet.* **2007**, 22, 225-254.
15. McAllister,M. Dynamic dissolution: A step closer to predictive dissolution testing? *Mol. Pharm.* **2010**, 7, 1372-1387.
16. *Pharmaceutical Dissolution Testing,* Eds. Dressman,J.;Krämer,J. Publisher: Informa healthcare,

London, England.2007
17. US Patent Apl. 2008/0138261 A1. Flow-through apparatus for microscopic investigation of dissolution pharmaceutical solids. R. Bogner et. al
18. Sugano,K. Aqueous boundary layers related to oral absorption of a drug: From dissolution of a drug to carrier mediated transport and intestinal wall metabolism. *Mol. Pharm.* **2010**, 7, 1362-1373.
19. Johnson, D.; Amidon, G. Determination of intrinsic membrane transport parameters from perfused intestine experiments: A boundary layer approach to estimating the aqueous and unbiased membrane permeabilities. *J. Theor. Biol.* **1988**, 131, 93-106.
20. Sugano, K. Theoretical comparison of hydrodynamic diffusion layer models used for dissolution simulation in drug discovery and development. *Int. J. Pharm.* **2008**, 363, 73-77.
21. D'Arcy, D.M.; Liu, B.; Bradley, G.; Healy, A.M.; Corrigan, O.I. Hydrodynamic and species transfer simulations in the USP 4 dissolution apparatus: Considerations for dissolution in a low velocity pulsing flow. *Pharm. Res.* **2010**, 27,246-258.
22. Fotaki, N.; Reppas, C. The flow through cell methodology in the evaluation of intralumenal drug release characteristics. *Diss. Tech*. **2005** May.